Automated segmentation of regions of interest on hand radiographs[a)]

Shirley N. C. Cheng,[b)] Heang-Ping Chan, Loren T. Niklason,[c)] and Ronald S. Adler
Department of Radiology, University of Michigan-Ann Arbor

(Received 29 September 1993; accepted for publication 11 May 1994)

Most radiologists do not use texture information contained in the trabecular patterns of hand radiographs to diagnose erosive changes and demineralization due to systemic inflammatory diseases that affect the skeletal system. However, high-resolution digitization achievable by a laser digitizer now makes it possible to access texture information that may not be perceived visually. We are studying the feasibility of computer-assisted early detection of these processes with particular attention to patients with hyperparathyroidism. In this paper the methods used to extract a region of interest (ROI) for texture analysis are discussed. The techniques include multiresolution sensing, automatic adaptive thresholding, detection of orientation angle, and projection taken perpendicular to the line of least second moment. The methods were tested on a database of 50 pairs of hand radiographs. We segmented the middle and the index fingers with an average success rate of 83% per hand. For the segmented finger strips, we located ROIs on both the middle and the proximal phalanges correctly over 84% of the times. Texture information was collected in the form of a concurrence matrix within the ROI. This study is a prelude to evaluating the correlation between classification based on texture analysis and diagnosis made by experienced radiologists.

Key words: hand radiograph, least second moment, adaptive thresholding, texture analysis

I. INTRODUCTION

Hand radiographs are used to assess the severity of disease in patients with hyperparathyroidism.[1] The features most commonly used by radiologists for early detection are the roughness of the lateral phalangeal margins and subperiosteal resorption of the terminal tufts as projected on the radiograph.[2,3] At present, information related to the texture of trabecular patterns is not used clinically as a major diagnostic factor. The human visual system is more sensitive to sudden changes in intensities such as an edge, rather than small variations that spread over a region, such as the case with texture.[4] This may partially explain the reason for lack of interest in using texture as a feature for detection.

With technological advances in high-resolution laser digitizers, very fine texture information can now be captured. High-resolution digitized radiographs make it possible for computers to access texture information that may not be perceived visually. Our preliminary study on texture analysis of trabecular patterns indicates that there is a correlation between the texture features and the severity of disease as determined by experienced radiologists.[5,6] The hand radiographs of a patient with hyperparathyroidism as shown in Fig. 1(a) is compared with a normal hand radiograph shown in Fig. 1(b). It is difficult to detect the differences in the texture between these two by visual inspection. However, matrices extracted from regions on the two radiographs reveal a distinctive difference. The matrices shown in Fig. 2 are called concurrence matrices by Jain,[7] cocurrence matrices by Rosenfeld and Kak,[8] and joint probability matrices by Pratt.[9] A more detailed discussion of this matrix will be included in a later section.

The success of texture analysis depends strongly on the fidelity of preservation of texture. In previous studies, the original images are typically rotated to align the longitudinal direction of the image with the vertical axis of the image matrix.[10] The algorithms that accomplish this task usually use interpolation to fill the "holes" resulting from rotating the coordinate system. In doing so, an equivalent low-pass filter is applied to the original high-resolution image, resulting in a loss in actual resolution. In the approach described in this paper, regions of interest (ROIs) are extracted directly from the original image to preserve texture information.

Another important issue in texture analysis is the large amount of data necessary for training and testing a classifier to ensure its ability to handle variability in data. Therefore, the collection of texture information in a consistent manner by the computer becomes the foremost important step in automated computer-aided detection of osteopenia. In this paper, we present the results of our study on automated segmentation of ROIs from hand radiographs for texture analysis. The method we developed includes the following steps.

(1) Multiresolution sensing: The high-resolution digital images are compressed to low-resolution images using Laplacian compact code. This step not only reduces the processing time but also blurs fine structures that are irrelevant to, or sometimes even interfering with, the extraction of ROI.

(2) Multisegment projections: Vertical and segmented vertical projections are taken. The maxima and minima on those projection profiles are detected using a zero crossing technique. A strip containing a finger is then segmented based on the locations of these zero crossings. Provisions are made for fingers that do not align with the vertical axis by trimming off excesses from neighboring fingers.

(3) Automatic adaptive thresholding: From the histogram plot of each finger strip, a zero crossing technique is again used to determine automatically the threshold levels for segmentation of the bone mass. This method provides the mechanism whereby threshold levels of radiographs obtained with a wide range of exposure levels may be selected adaptively on a case-by-case basis.

(4) Automatic detection of orientation: A technique of the least second moment is used to locate the line that passes

 0094-2405/94/21(8)/1293/8/$1.20

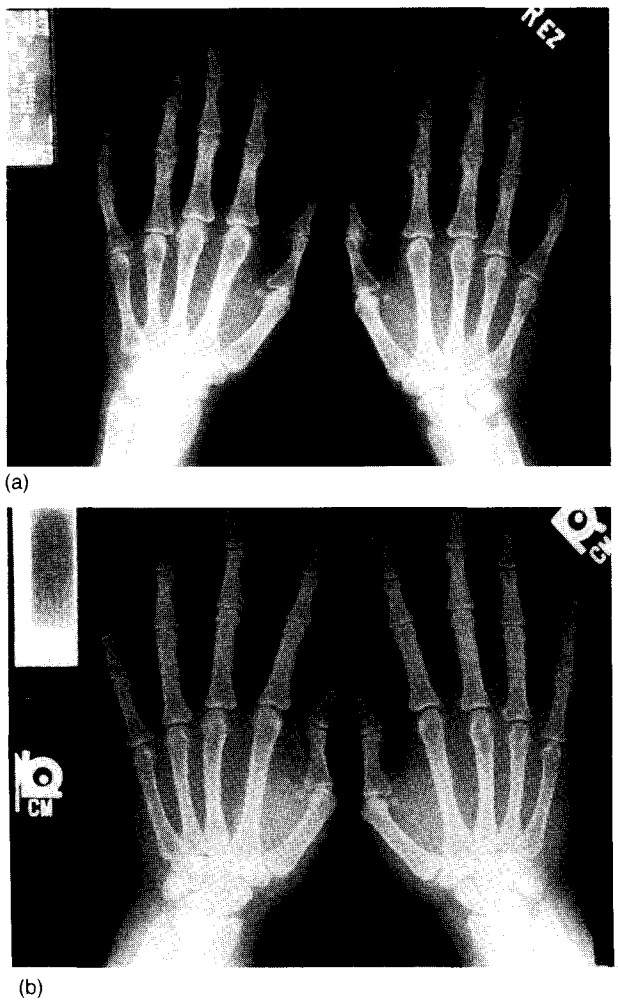

FIG. 1. Hand radiographs of (a) a patient with hyperparathyroidism and (b) a normal person.

through the center of the bone mass and has the same orientation as the longitudinal axis of the phalanx. A projection is then taken along the axis perpendicular to the axis of the least second moment. Position information about the middle and proximal phalanges are inferred from the signatures on the projection profile.

II. METHODS

A. Selection of ROI

The concurrence matrix is an estimate of the joint probability density function of gray levels at two different locations (pixels) on the image. A selection rule specifies the relative direction and distance of the pixel pairs. To estimate the joint probability density function, we obtain a two-dimensional histogram whose vertical and horizontal axes are quantized gray levels. The values of this two-dimensional array are the cumulative sum of the number of pixel pairs whose gray levels correspond to the indices in the concurrence matrix. The matrix shown in Fig. 2 is an example of a two-dimensional histogram. The concurrence matrix, as defined in the literature,[7–9] is a normalized version of this histogram.

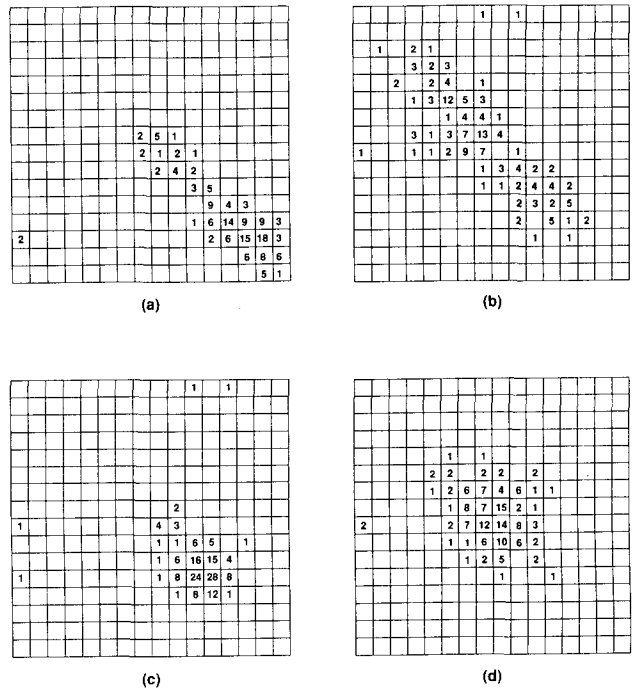

FIG. 2. Concurrence matrices obtained from the middle fingers of images shown in Fig. 1: (a) abnormal proximal phalanx; (b) abnormal middle phalanx; (c) normal proximal phalanx; and (d) normal middle phalanx.

The selection rule plays an important role in deciding the type of texture information to be collected.[9] We choose to compare pixels along the center line of the phalanx and lines parallel to it. This choice is based on the assertion that the texture patterns are parallel to the median of the phalanx, and the coarseness of these patterns is correlated to bone mineral density. The distance between the two parallel lines is a parameter which depends upon the resolution of the digitized image.

The early manifestations of demineralization are most pronounced in the middle and proximal phalanges of the index and middle fingers. To gather as much information as possible to have a meaningful statistical interpretation, while maintaining manageable computational complexity, the ROI is selected as a rectangular window consisting of 40×160 pixels. The ROI is located within each phalanx in the region of cancellous bone, aligned with the longitudinal axis of the phalanx. The concurrence matrices in Fig. 2 are extracted from the ROIs on the middle and proximal phalanges of the middle finger. Every other pixel along the center line is compared with pixels along parallel lines about 0.2 mm away from the center line. In the following section, we discuss in detail the techniques used and illustrate how these techniques may be combined to achieve the following objectives: (1) automatic separation of the left and right hands; (2) automatic segmentation of strips that contain the middle and the index fingers, respectively; (3) automatic placement of two windows along the longitudinal axis of the middle and proximal phalanges; and (4) collection of texture information from these two windows.

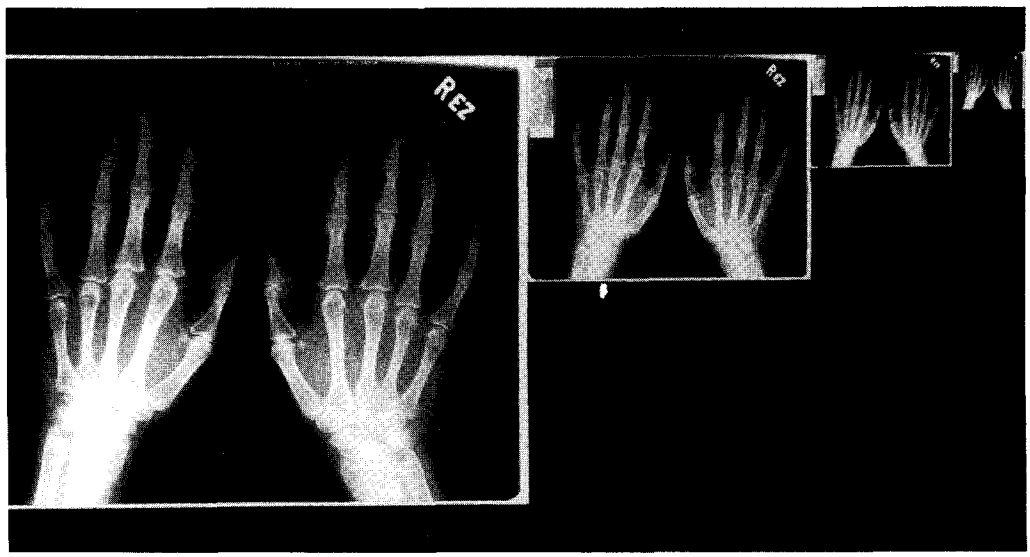

FIG. 3. Laplacian pyramid images. From left to right: level-zero (3000×2400 pixels, 0.1 mm/pixel), level-one (1500×1200 pixels, 0.2 mm/pixel), level-two (750×600 pixels, 0.4 mm/pixel), level-three (375×300 pixels, 0.8 mm/pixel).

B. Multiresolution sensing

To preserve the detailed texture information, radiographs recorded by a screen-film system are digitized by a LUMISYS high-resolution laser digitizer. The radiographs are digitized at a pixel size of 0.1×0.1 mm and 12-bit quantization levels. The high resolution resulted in a digital image of 3000×2400 pixels and 14.4 Mbytes of memory space, when the 12-bit quantized levels are stored as a two-byte integer. To reduce the processing time, as well as to blur fine structures that may otherwise interfere with the detection of ROIs, the images are compressed to a size of 375×300 pixels using the Laplacian pyramid.

The Laplacian pyramid has a wide range of applications, especially in image compression and progressive image transmission. Burt and Adelson[11] described how classification could be accomplished by first searching within a low-resolution image and then proceeding to a region within a high-resolution image for more detailed features. This multiresolution search method is similar to that observed in a human vision system where the retina processes coarse structural information at a lower resolution and then zooms in to a region of finer resolution.[4]

We implemented the Laplacian pyramid based on an algorithm described by Burt and Adelson.[11] The lower level resolution image is obtained by first convolving the higher resolution image with a 5×5 window. The window is a Gaussian-like two-dimensional mask, separable in the horizontal and vertical directions. The image size is reduced to one quarter of the original size by retaining only every other pixel. This process is similar to down sampling except for the additional process of first convolving the image with a window, which is essentially a low-pass filter, thereby preventing aliasing that may occur during down sampling.

Images of four different resolutions in the Laplacian pyramid are shown in Fig. 3. The one on the left is the original level-zero image and the one on the right is the level-three image, which is the level used in the ROI detection described below.

C. Vertical projections

A vertical projection is defined as the sum of pixel values along the vertical lines. Figure 4(a) is a profile of the vertical projection of the hand radiograph shown in Fig. 1(a). The high projection value near the left is due to the patient label at the upper left corner. The extremely high projection value on the right corresponds to the white edge. The low projection value near the center signifies the dark background area separating the two hands. These characteristics are used to trim the edges and separate the left and right hands.

To extract the middle and index fingers from a hand, we use segmented projections. Figure 4(b) is a projection taken from the top of the left-hand image to one quarter from the top. Only three maxima appear and they correspond to the tips of the index, middle, and fourth fingers. Figure 4(c) is a projection taken from the top one quarter to the top half of the image. Five maxima appear in this projection profile. The two additional maxima correspond to the thumb and the little finger.

There are advantages of using projection instead of edge detection techniques. Taking the projection of an image is an integration operation whereas edge enhancement techniques are generally differentiation operations. A differentiator is a high-pass filter and it amplifies high-frequency noises that are commonly present in radiographs. An integrator is a low-pass filter and it averages out random noises.

The above-mentioned techniques may fail if there are interferences with the basic profile. This occurs when there are large patient identification labels or lead markers placed on top of the fingers. In addition, when the hands are oriented at exceptionally large angles with respect to the vertical axis, or when all the fingers are in contact with one another, the

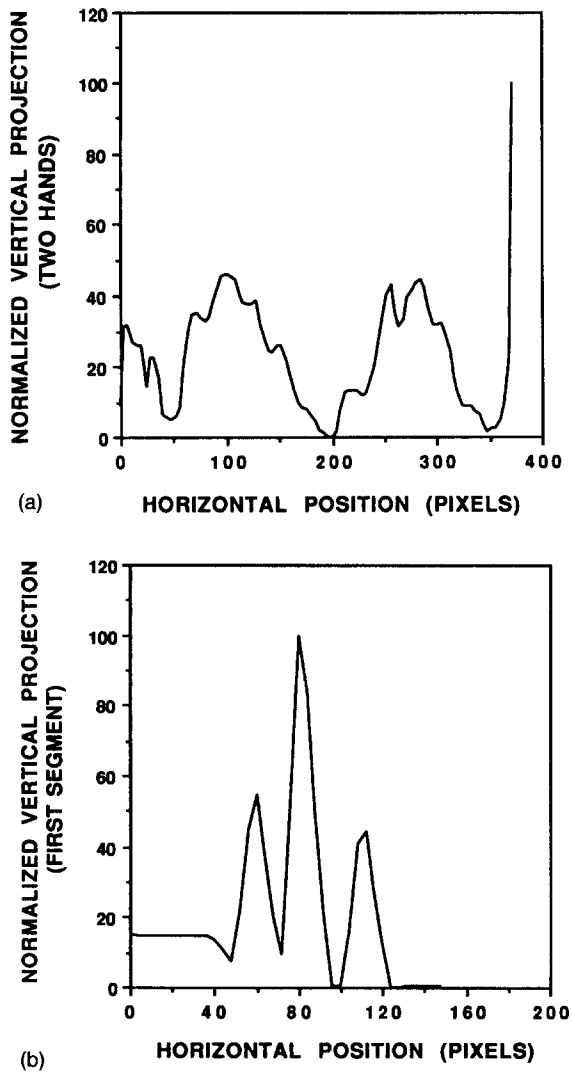

FIG. 4. Normalized vertical projections of the image shown in Fig. 1(a): (a) the two hands; (b) the first segment of left hand; and (c) the second segment of left hand. Each pixel along the horizontal axis corresponds to a distance of 0.8 mm on the hand radiograph.

projection profile becomes flat and no maxima or minima can be detected.

D. Zero crossing

To accurately locate the maxima and minima on the projection profile, the forward differences of the projection values are taken. A smoothed version of the difference is obtained by convolving the difference with a Gaussian kernel to smooth out the undesirable peaks due to noises. The zero crossings of the smoothed difference correspond to the locations of maxima and minima, which are related to the positions of different fingers. To detect the zero crossings we implemented an algorithm described by Kunt, Ikonomopoulos, and Kocher.[12] The algorithm searches for a pair of positive and negative first derivatives of the profile and determines if that corresponds to a zero crossing.

A logical operation on the magnitude of the projection profile at each zero crossing and their neighbors determines which of these crossings are minima and which are maxima. We also detect the position of continuous runs of zero values. Positions of each finger strip are determined by logical operations on the information. The finger strips shown in Fig. 5 are obtained by detecting the minima of the smoothed profile difference. Some of the finger strips, such as the middle finger of the left hand, contain small portions of the neighboring fingers. This usually happens when the fingers are not aligned with the vertical axis, or when the fingers are in contact with each other. These excesses are trimmed by the following procedures.

E. Automatic adaptive thresholding

It is necessary to segment out the bone mass for accurate determination of the longitudinal axis of a phalanx. The zero-crossing detection technique is also used in automatic adaptive thresholding. The histogram of the finger strip shown in Fig. 5(a) is plotted in Fig. 6. The histogram is approximately a trimodal Gaussian distribution. The peak on the left corresponds to the background, the peak at the center is the soft tissue, and bone masses contribute to the peak on the right. Michael and Nelson[13] estimated the mean and the variance of such distributions and selected a fixed threshold level to segment out the bone masses. We differ from their approach in that we determine the threshold levels for each radiograph based on each individual histogram. In a sense, this is a "true" adaptive method when the threshold level is selected on a case-by-case basis. This method is particularly suited for histograms that have distinctive peaks and valleys. The method fails, however, when the radiographs are excessively over- or under-exposed.

(a)

(b)

FIG. 5. Segmented finger strips of the hands in Fig. 1(a): (a) middle finger of left hand; (b) index finger of left hand; (c) middle finger of right hand (mirror image); and (d) index finger of right hand (mirror image).

Again, the forward difference of the histogram profile is taken and convolved with a smoothing Gaussian kernel. The smoothed version is then subjected to zero-crossing detection. The zero crossing corresponding to the first minimum from the high-intensity-level end of the histogram determines the threshold level that segments out the bone masses. The image in Fig. 7(a) is a result of applying the automatic adaptive thresholding method to the image in Fig. 5(a). Notice that the soft tissue of the finger strip and a portion of the neighboring fourth finger disappear.

To trim off the remaining small portion of bone mass of the adjacent index finger, four segmented vertical projections are taken. Positions of maxima, minima, and continuous runs of zeros are found. There should be one distinctive maximum value for each segmented projection. The excess portion of neighboring fingers is then trimmed based on the locations of the secondary maxima, as shown in Fig. 7(b).

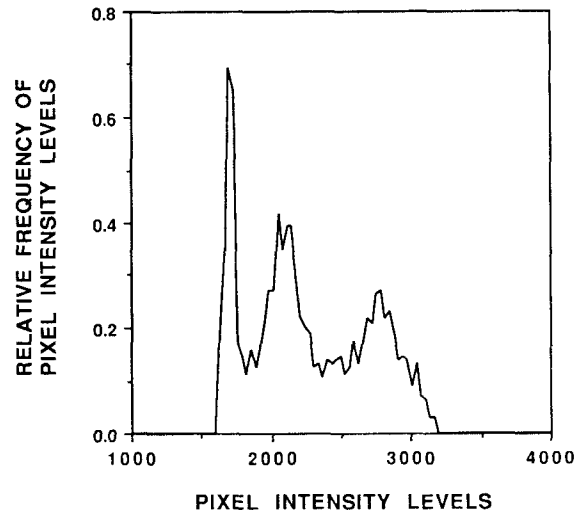

FIG. 6. Histogram of the finger strip shown in Fig. 5(a).

F. Orientation through the least second moment method

To locate a region on a finger, it is necessary to first determine the line that passes through the center of bone mass with the same orientation as the phalanx. Horn used binary images to calculate the line of the least second moment as a way of determining the angle of orientation.[14] We modify his method for application to gray level images. The following equations were derived to find the center of mass (x_0, y_0) and the angle of orientation θ for the axis of least second moment, defined with respect to the horizontal axis.

$$\theta = \frac{1}{2} \tan^{-1}\left(\frac{2\rho_{xy}}{\sigma_x^2 - \sigma_y^2}\right), \tag{1a}$$

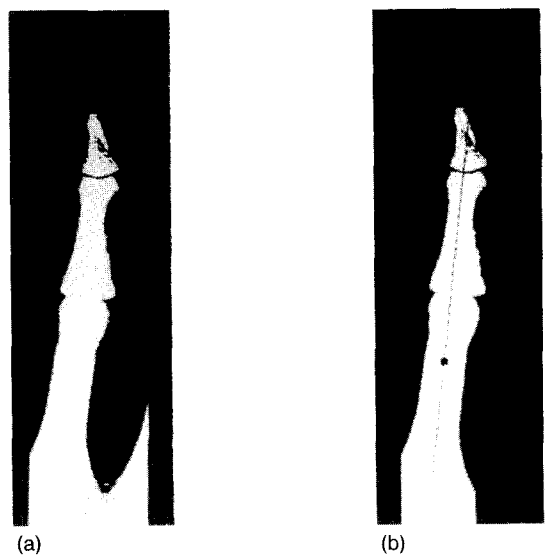

(a) (b)

FIG. 7. (a) Threshold segmentation of finger strip shown in Fig. 5(a). Notice that the soft tissue of the finger strip and the portion of the fourth finger disappear. (b) The excess of the index finger is trimmed. The center of mass and axis of the least second moment are superimposed on the trimmed image.

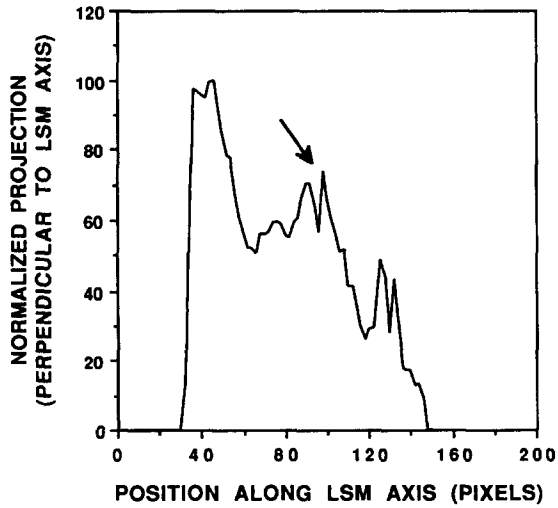

FIG. 8. Projection taken perpendicular to the axis of least second moment. The arrow points to the position corresponding to the joint between the middle and proximal phalanges. Each pixel along the horizontal axis corresponds to a distance of 0.8 mm on the hand radiograph.

$$x_0=\frac{1}{C}\sum_{i=0}^{N_x-1}\sum_{j=0}^{N_y-1}\left(i-\frac{N_x}{2}\right)f_{ij}\,, \tag{1b}$$

$$y_0=\frac{1}{C}\sum_{i=0}^{N_x-1}\sum_{j=0}^{N_y-1}\left(j-\frac{N_y}{2}\right)f_{ij}\,, \tag{1c}$$

where

$$\sigma_x^2=\frac{1}{C}\sum_{i=0}^{N_x-1}\sum_{j=0}^{N_y-1}(i-[x_0])^2 f_{ij}\,, \tag{1d}$$

$$\sigma_y^2=\frac{1}{C}\sum_{i=0}^{N_x-1}\sum_{j=0}^{N_y-1}(j-[y_0])^2 f_{ij}\,, \tag{1e}$$

$$\rho_{xy}=\frac{1}{C}\sum_{i=0}^{N_x-1}\sum_{j=0}^{N_y-1}\left(i-\frac{N_x}{2}\right)\left(j-\frac{N_y}{2}\right)f_{ij}\,, \tag{1f}$$

$$C=\sum_{i=0}^{N_x-1}\sum_{j=0}^{N_y-1}f_{ij}\,, \tag{1g}$$

where f_{ij} is the pixel value at the (i,j) pixel, and N_x and N_y are the number of pixels along x and y directions, respectively. In Fig. 7(b), the axis of least second moment and the center of mass are superimposed on the trimmed image. For this image, the center of mass is located at $(-4.44, -30.9)$, with respect to the center of the 48×150-pixel level-3 finger strip image array. The orientation angle is 83.44 degrees.

G. Automatic extraction of ROI

The profile shown in Fig. 8 is a projection taken perpendicular to the axis of least second moment. The notches on the projection profile correspond to the joints on a finger. The higher projection values at both the left and the right of the notch correspond to the enlarged areas surrounding the joint.

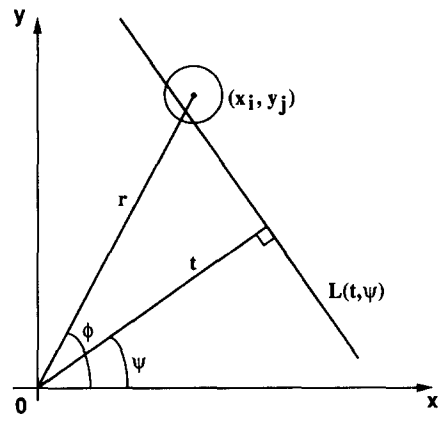

FIG. 9. Coordinate system for a projection along a line.

Locations of the middle and proximal phalanges can then be inferred from these signatures. In order to obtain this projection profile, we derived an expression to efficiently evaluate the projection perpendicular to the axis of least second moment.

A projection line $L(t,\Psi)$ is defined by the view angle Ψ and the translation distance t as shown in Fig. 9. A projection $p(t,\Psi)$ is an integration of the pixel values $f(x,y)$ along the line $L(t,\Psi)$. Mathematically, a projection is expressed as

$$p(t,\Psi)=\int_{L(t,\Psi)}f(x,y)dl$$
$$=\int_{-\infty}^{\infty}f(t\cos\Psi-u\sin\Psi,t\sin\Psi+u\cos\Psi)du. \tag{2a}$$

For digitized images, $f(x,y)$ is assumed to be piecewise constant within each pixel, and the projection may be approximated as

$$p(t,\Psi)=\sum_{(i,j)\ \text{along}\ L(t,\Psi)}W_{ij}f_{ij}\,, \tag{2b}$$

where f_{ij} is the pixel value at the (i,j)th pixel and W_{ij} is the weighting function, and the summation is performed over pixels along the projection line.

For the convenience of arriving at a closed-form expression of the weighting function, a circular pixel of radius δ is assumed. The center of the circular pixel is defined by the polar coordinates as shown in Fig. 9. For the purpose of clearer illustration, the pixel is not drawn to scale. The contribution of each pixel to the total projection value is determined by the length of intersection between the projection line and the circular pixel. Therefore, the weighting function is equal to

$$W_{ij}=2\sqrt{\delta^2-d^2},\quad \text{for } \delta>d;$$
$$0,\quad \text{otherwise.} \tag{2c}$$

where

$$d=t-r\cos(\phi-\Psi)=t-(x_i\cos\Psi+y_j\sin\Psi) \tag{2d}$$

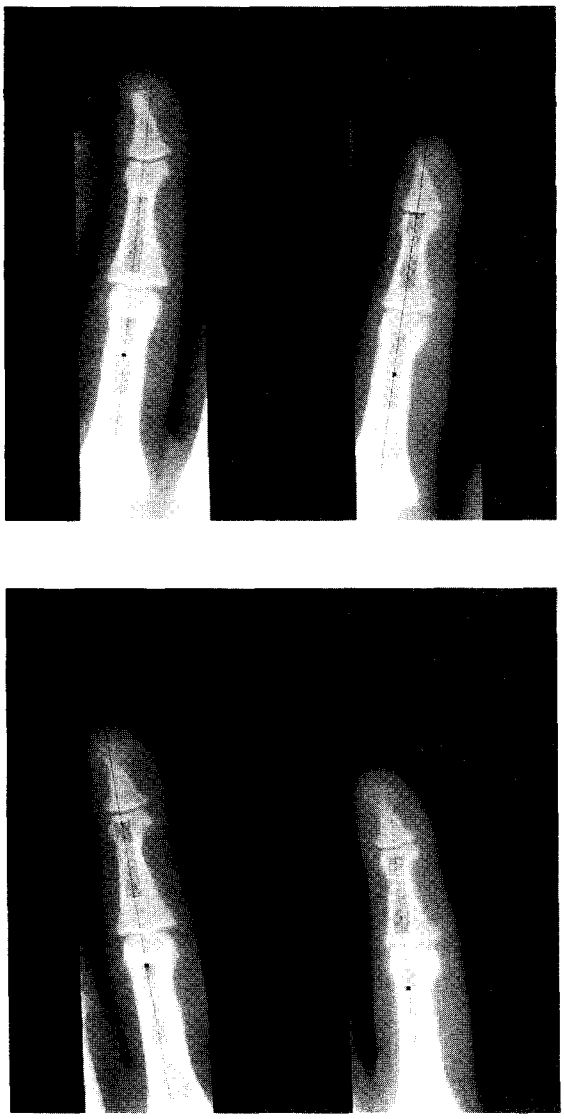

FIG. 10. Location of ROIs superimposed on the four phalanges shown in Fig. 5.

and (x_j, y_j) is the rectangular coordinate of the center of the (i,j)th pixel.

The projection algorithm was tested on several standard computer-simulated test images such as lines with different orientations. The error in the projection value, due to approximating a square pixel by a circular pixel, was found to be between 0% and 8%, depending upon the relative orientation of the projection line. The error is tolerable for our purpose.

The locations of the notches on the projection profile corresponds to the zero crossings of the forward differences of the projection values. The middle phalanx is located between the second and the third crossings, and the proximal phalanx is located between the third crossing and the bottom edge. With this information in place, the positions of the ROIs on the level-3 image can be determined. The positions of these ROIs are then translated to positions on the original level-zero image to extract high-resolution ROIs. In Fig. 10, each finger strip shown in Fig. 5 is overlayed with two boxes indicating the locations of the ROIs determined for the middle and the proximal phalanges.

III. RESULTS

We tested the procedures described in the previous sections on a data base consisting of 50 pairs of hand radiographs. The data set did not include hands having exceptionally large orientation angles or having fingers that were extremely tightly placed. The procedures successfully separated the left hand 100% of the times but only 76% for the right hand. The failed cases were due to large patient identification labels placed near or, in some cases, in contact with the right wrist, causing the small finger to be cut off. The right-hand segmentation rate could have increased to 100% if these cases were discarded.

Of the correctly segmented hands, the procedures successfully extracted 82% of the middle fingers and 90% of the index fingers for the left hand. The correct segmentation rates were 82% and 79%, respectively, for the right hand. The average segmentation rate, therefore, was 83%. We found that, in some cases, the presence of lead markers used for identification of the left or right hands in the areas above the fingers misled the computer programs. In other cases the patient identification labels were placed above the little finger. These markers and labels distorted the characteristic signatures of the projection profiles. However, the problem can be readily avoided if x-ray technologists are instructed to place the labels in designated areas away from the patient's hands. The segmentation rates will increase if cases with prominent markers or labels in the critical regions of the image are not present.

A total of 147 segmented finger strips were used for testing the automatic extraction of ROI along the longitudinal axis of phalanges. A finger strip was deemed usable if it contained only one finger and perhaps only a small portion of another finger. We found that 84% of the times, the ROIs were identified correctly on both the middle and the proximal phalanges. When the finger strip contained a significant portion of a neighboring finger, the method failed. The success rate of this step was dependent upon how well the fingers were segmented as well as how effective the adaptive thresholding method was in isolating the bone masses. Most of the failed cases were due to interferences caused by partial neighboring fingers. Some were caused by incorrect threshold levels. The results of successful segmentation rate are summarized in Table I.

IV. DISCUSSION

To quantify the difference between normal and abnormal cases, we evaluate the inertia and the moments of a concurrence matrix associated with the ROIs. Our preliminary results indicate that there are differences in these quantities which may be used for classification of the normal and the abnormal cases. In order to make a definitive conclusion about the correlation between these texture features and the degree of severity of mineral resorption, a large sample of data is required for training and testing. The data collection will be a very tedious process if it is done manually. The

TABLE I. Segmentation success rate.

Hand Segmentation (Average: 88%)		
Two-hand image	Left hand	Right hand
50	50 (100%)	38 (76%)

Finger strip segmentation (Average: 83%)			
	Single hand	Middle finger	Index finger
Left hand	50	41 (82%)	45 (90%)
Right hand	38	31 (82%)	30 (79%)
Total	88	72 (82%)	75 (85%)

ROI Segmentation (Average: 84%)		
	Fingerstrips	ROI on both middle and proximal
Left-hand middle finger	41	35(85%)
Left-hand index finger	45	36(80%)
Right-hand middle finger	31	26(84%)
Right-hand index finger	30	27(90%)
Total	147	124(84%)

techniques outlined in the previous discussion are used to accomplish this task automatically by a computer so that we can collect texture information in a consistent manner. Automation of texture information collection is critical to the success of computer-aided diagnoses of mineral resorption and bone loss, if it is to be implemented for clinical applications.

A major factor affecting our success rate in this study is the interference with the projection profiles by patient identification labels and lead markers placed too close to the fingers. For future studies, we suggested that a radiation transparent template overlaying the cassette be used for the patients to align their finger placements, and for the technologists to place the markers and labels. This approach will also eliminate the occurrence of hand images with exceptionally large orientation angles or having fingers that are extremely tightly placed.

V. CONCLUSION

We demonstrated the use of multiresolution sensing, projection along a line, zero-crossing detection, automatic adaptive thresholding, and the least second moment technique to locate ROIs on hand radiographs. Once the ROI is segmented, we can then collect texture information by way of a concurrence matrix. Features such as inertia and moments are evaluated to quantify the differences in texture coarseness. We are in the process of implementing an artificial neural network classifier for texture discrimination. The success of a classifier depends largely on how well the statistical properties of the data are. A large training set is essential to ensure the versatility of this classifier. The procedures described in this paper pave the way for implementing a reliable classifier by providing techniques for automated texture information gathering so that a large amount of training data can be collected in a fast and consistent manner. The issue of texture classification using artificial neural networks will be addressed in future studies.

ACKNOWLEDGMENTS

The authors thank Diane Williams for typing the manuscript, Dr. Daniel St. Clair of University of Missouri Engineering Center for his efforts in computing facility support, and Chair-Li Chang of the Bioengineering Program at University of Michigan at Ann Arbor for collecting the hand radiographs. This work was supported in part by USPHS Grant No. CA48129.

[a]Please address all correspondence to Heang-Ping Chan, Ph.D., Department of Radiology, University of Michigan Hospitals, Taubman Center 2910, 1500 E. Medical Center Drive, Ann Arbor, Michigan 48109-0326; Phone: (313) 936-4357; Fax: (313) 936-9723.

[b]Current address: AccessAnywhere Communication, Inc., P.O. Box 11884, St. Louis, Missouri 63105.

[c]Current address: Radiological Sciences and Technology, Massachusetts General Hospital, Boston, Massachusetts 02114.

[1]D. Resnick, L. J. Deftos, and J. G. Parthemore, "Renal osteodystrophy: magnification radiography of target sites of absorption," Am. J. Radiol. **136**, 711–714 (1981).

[2]C. L. Chang, H. P. Chan, S. N. C. Cheng, L. T. Niklason, R. S. Adler, M. Cobby, and J. Crabbe, "Computer-aided detection of skeletal changes in hyperparathyroidism," The Society for Imaging Science and Technology 44th Annual Conference, Paper Summaries, pp. 377–380, St. Paul, MN, May 1991.

[3]C. L. Chang, H. P. Chan, L. T. Niklason, M. Cobby, J. Crabbe, and R. S. Adler, "Computer-aided diagnosis: Detection and characterization of hyperparathyroidism in digital hand radiographs," Med. Phys. **20**, 983–992 (1993).

[4]K. T. Spoehr and S. W. Lehmkuhle, *Visual Information Processing* (W. H. Freeman, San Francisco, CA, 1982).

[5]S. N. C. Cheng, H. P. Chan, R. S. Adler, L. T. Niklason, and C. L. Chang, "Development of a neural network, for early detection of renal osteodystrophy," Proc. Int. Soc. Opt. Eng. **1450**, 90–98 (1991).

[6]S. N. C. Cheng, H. P. Chan, L. T. Niklason, R. S. Adler, and C. L. Chang, "Texture analysis of trabecular patterns on phalanges using neural network," Radiology **181**, 143 (1991).

[7]A. K. Jain, *Fundamentals of Digital Image Processing* (Prentice-Hall, Englewood Cliffs, NJ, 1989).

[8]A. Rosenfeld and A. Kak, *Digital Picture Processing* (Academic, New York, NY, 1982), Vol. 2.

[9]W. K. Pratt, *Digital Image Processing* (Wiley, New York, 1978).

[10]E. Pietka, M. F. McNitt-Gray, M. L. Kuko, and H. K. Huang, "Computer-assisted phalangeal analysis in skeletal age assessment," IEEE Trans. Medical Imaging **10**, 616–620 (1991).

[11]P. J. Burt and E. H. Adelson, "The Laplacian pyramid as a compact image code," IEEE Trans. Commun. **1**, 532–540 (1983).

[12]M. Kunt, A. Ikonomopoulos, and M. Kocher, "Second generation image coding techniques," Proc. IEEE **73**, 549–574 (1985).

[13]D. J. Michael and A. C. Nelson, "Handx: A model-based system for automatic segmentation of bones from digital hand radiographs," IEEE Trans. Medical Imaging **8**, 64–69 (1989).

[14]B. K. P. Horn, *Robot Vision* (MIT, Boston, 1986).